# SCIENTIFIC REP🞰RTS

**OPEN**

# Lagrangian Statistics and Intermittency in Gulf of Mexico

Liru Lin[1], Wei Zhuang[2] & Yongxiang Huang[2]

Due to the nonlinear interaction between different flow patterns, for instance, ocean current, meso-scale eddies, waves, etc, the movement of ocean is extremely complex, where a multiscale statistics is then relevant. In this work, a high time-resolution velocity with a time step 15 minutes obtained by the Lagrangian drifter deployed in the Gulf of Mexico (GoM) from July 2012 to October 2012 is considered. The measured Lagrangian velocity correlation function shows a strong daily cycle due to the diurnal tidal cycle. The estimated Fourier power spectrum $E(f)$ implies a dual-power-law behavior which is separated by the daily cycle. The corresponding scaling exponents are close to $-1.75$ and $-2.75$ respectively for the time scale larger (resp. $0.1 \leq f \leq 0.4 \, \mathrm{day}^{-1}$) and smaller (resp. $2 \leq f \leq 8 \, \mathrm{day}^{-1}$) than 1 day. A Hilbert-based approach is then applied to this data set to identify the possible multifractal property of the cascade process. The results show an intermittent dynamics for the time scale larger than 1 day, while a less intermittent dynamics for the time scale smaller than 1 day. It is speculated that the energy is partially injected via the diurnal tidal movement and then transferred to larger and small scales through a complex cascade process, which needs more studies in the near future.

The movement of the ocean is extremely complex due to the nonlinear interaction between different flow patterns, where turbulence may play an important role[1]. For instance, the energy could injected to the system via the instability of the ocean current with a length scale hundreds or thousands kilometers and then transferred to the so-called mesoscale eddies through a possible cascade process. A better understanding of this process is crucial for not only the ocean dynamics, but also an ideal testbed with high Reynolds numbers for turbulence theory[2]. The Gulf of Mexico (GoM) is such a typical region exhibiting a very complex dynamics, such as Loop Current (LC), diurnal tide, mesoscale and sub-mesoscale eddies, etc, see an illustration in Fig. 1. It is a semi-enclosed marginal sea located west of the Atlantic Ocean, connected with the Atlantic Ocean to the east via the Florida Straits and the Caribbean Sea to the south via the Yucatan Channel. The GoM circulation is characterized by strong current possessing notable variability. The LC is the most energetic components of ocean circulation in the GoM and significantly affect multi-scale processes herein. It originates from the northward-flowing Yucatan Current. After passing through the Yucatan Channel, the LC circulates anticyclonically in the eastern GoM and then exits through the Florida Straits[3,4]. Within the GoM, the LC displays a wide range of spatiotemporal variability and episodically sheds anticyclonic rings, which are ~300 km in diameter and ~1000 m in vertical extent[3–7]. The time interval between the ring shedding events varies from a few weeks to 19 months[8–10] with a mean period of about 8 months[11,12]. Besides the large warm-core rings, relatively smaller-scale frontal eddies and filaments are also observed around the edges of LC and its rings by *in-situ* and remote sensing data, indicating the active mesoscale and sub-mesoscale variability in the GoM[13–15]. Meanwhile, the LC's impact could also extends to the deep ocean, exciting topographic waves and bottom-intensified cyclonic eddies beneath the anticyclonic rings[16–18]. Numerical studies indicates that the LC-topography interactions and ring shedding are both in favor of the formation and development of cyclonic eddies, during which cyclones primarily gain energy from LC as a consequence of mean-to-eddy energy conversion[18–20]. The northeastern GoM is characterized by complex bathymetry, with a right-angle submarine valley, named the DeSoto Canyon, between two wide shelves (the West Florida Shelf and the Mississippi-Alabama Shelf). In this region, the local winds, eddy activities, topographic waves and Mississippi River input could jointly influence the interplay between the shelf and deep circulations, thus resulting in notable cross-shelf exchanges[21–24]. The LC rarely extends sufficiently northward to the DeSoto Canyon region. But it exerts indirect impacts on the shelf-slope flows around this region through either its associated eddies or the coastal-trapped waves exited by its impingement on the West Florida Slope[24–26]. The multiscale or

[1]South China Sea Institute of Planning and Environmental Research, State Oceanic Administration, Guangzhou, 510300, PR China. [2]State Key Laboratory of Marine Environmental Science & College of Ocean and Earth Sciences, Xiamen University, Xiamen, 361102, PR China. Correspondence and requests for materials should be addressed to W.Z. (email: wzhuang@xmu.edu.cn)
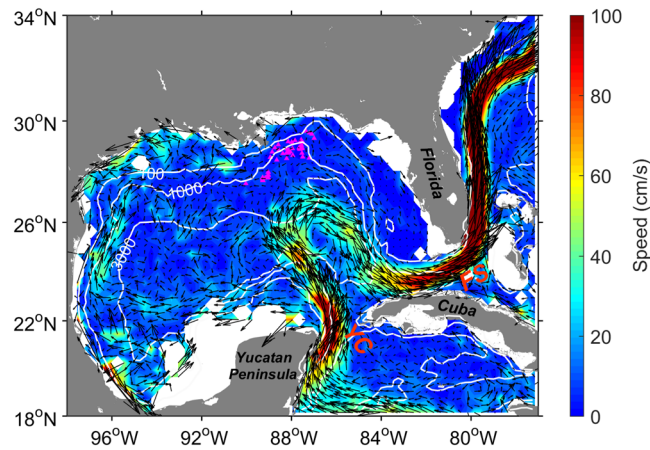
**Figure 1.** Mean sea surface current in the Gulf of Mexico averaged within 0.3° × 0.3° bin from the 2000–2016 Global Drifter Program trajectory dataset. White lines show the 100, 1000 and 3000 m isobaths. Purple triangles indicate the initial positions of the drifters deployed during the GLAD program. YC and FS represent the Yucatan Channel and the Florida Straits respectively. Figure is plotted using MATLAB R2014b (http://www.mathworks.com/) with the MMap (a mapping package, http://www.eos.ubc.ca/~rich/map.html).
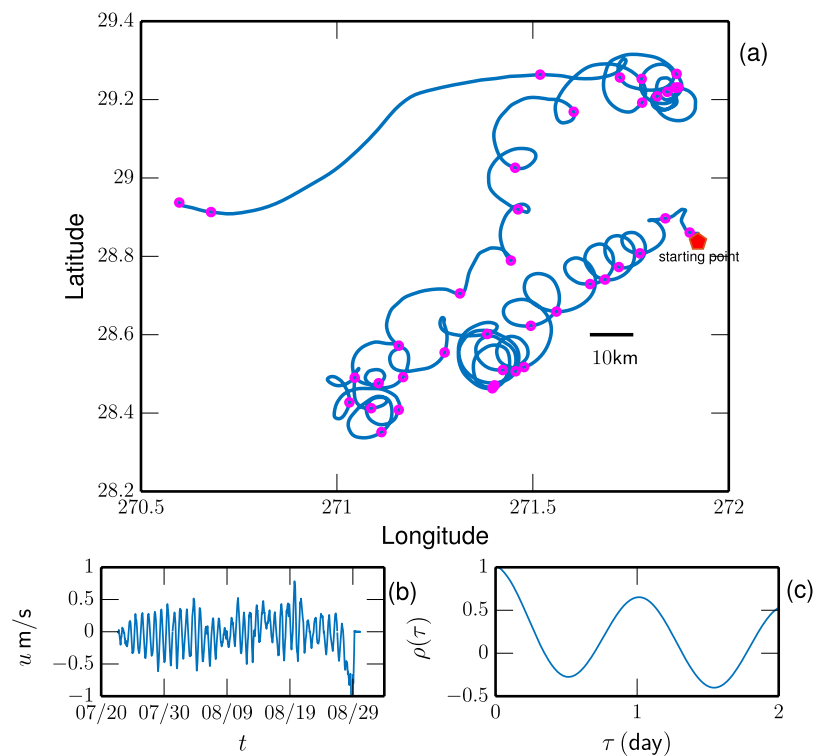


**Figure 2.** (**a**) Illustration of a 38 day trajectory of Lagrangian drifter on the time period 22th Jul. to 30th Aug. 2012. The 1 day time interval is indicated by symbols. (**b**) The corresponding Lagrangian velocity. (**c**) The measured Lagrangian correlation function $\rho(\tau)$, showing a strong daily cycle due to the tide. This figure is prepared using a Python package, namely Matplotlib.

scaling property of the ocean movement in GoM region has seldom been investigated. For example, the influence of the sub-mesoscale on two-drifter dispersion has been studied, where the Richardson-Obukhov scaling has been reported for the GLAD (Grand LAgrangian Deployment) experiment[27]. A Kolmogorov-like scaling in space for the second-order Eulerian structure-function is obtained from the same Lagrangian drifter experiment[28].

## Results

**Autocorrelation function and Fourier power spectrum.** Figure 2 (a) shows a 38 days long trajectory of Lagrangian drifter, where the symbol indicates the time interval 1 day, and (b) the corresponding zonal velocity
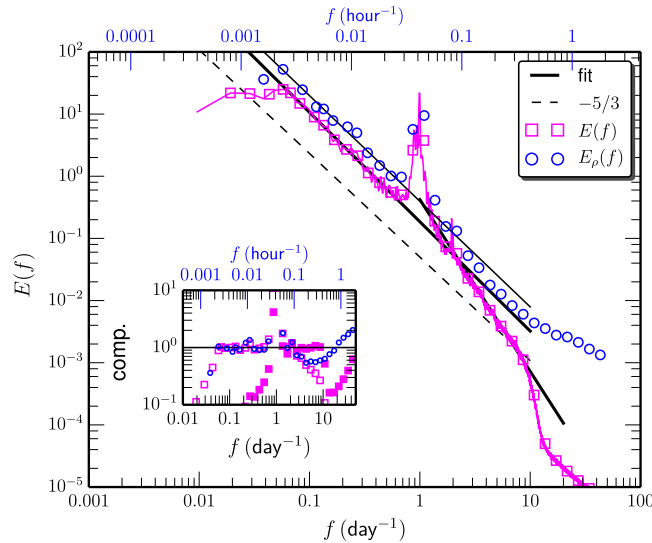
**Figure 3.** Measured Fourier power spectrum $E(f)$ provided by padding zeros and autocorrelation function (denoted as $E_\rho(f)$). Power-law behavior is observed on the range $0.06 \leq f \leq 0.6$ day$^{-1}$, and $2 \leq f \leq 8$ day$^{-1}$ respectively with scaling exponent $\beta_L^F = 1.75 \pm 0.08$ (resp. $\beta_{\rho,L}^F = 1.68 \pm 0.10$) and $\beta_S^F = 2.75 \pm 0.3$. For reference, the Kolmogorov $-5/3$ scaling for Eulerian velocity is shown as dashed line. For display clarity, the spectrum curve has been vertical shifted. The inset shows the compensated curve to emphasize the observed power-law behavior. This figure is prepared using a Python package, namely Matplotlib.

$u(t)$. Graphically, the daily cycle due to the diurnal tide is evidenced. To show this more clearly, the autocorrelation $\rho(\tau)$ is estimated, see 2 (c), where a strong daily cycle is visible. Figure 3 displays the measured Fourier power spectrum $E(f)$ by padding zeros to have the same length for each drifter ($\square$) and by applying the Wiener-Khinchin theorem to measured autocorrelation function $\rho(\tau)$ (denoted as $E_\rho(f)$, $\bigcirc$). Power-law behavior is observed for $E(f)$, e.g., $E(f) \propto f^{-\beta}$ on the range $0.05 \leq f \leq 0.5$ day$^{-1}$ and $2 \leq f \leq 8$ day$^{-1}$, corresponding to a time scale range $2 \leq \tau \leq 20$ day and $3 \leq \tau \leq 12$ hour. The measured scaling exponents are $\beta_L^F = 1.75 \pm 0.08$ and $\beta_S^F = 2.75 \pm 0.30$, where $F$ presents for the Fourier power spectrum, $L$ for the time scale larger than 1 day, and $S$ for the time scale smaller than 1 day. The inset shows the compensated curve to emphasize the observed scaling behavior. A statistical test shows that the padding zeros method overestimate the scaling exponent $\beta_L$ (not shown here). The second approach detects power-law behavior for the first scaling range, i.e., $0.05 \leq f \leq 0.5$ day$^{-1}$ with a scaling exponent $\beta_L^\rho = 1.68 \pm 0.10$. While the statistical test shows that the second scaling is biased. Both approaches predict a scaling exponent close to the Kolmogorov $-5/3$ for the low frequency part. Note that the Kolmogorov-Landau theory predicts a power-law behavior $E(f) \sim f^{-2}$ for the three-dimensional homogeneous and isotropic turbulence[29]. This type scaling has been reported for zonal and meridional velocity[30]. However, due to the existence of the strong diurnal tide, the measured $q$th-order Lagrangian structure-function, e.g., $S_q(\tau) = \langle |u(t + \tau) - u(t)|^q \rangle_t$ fails to detect the corresponding power-law behavior[28]. Therefore, whether the scaling range possesses intermittency correction or not can not be distinguished via the conventional approaches, such as structure-function, detrended fluctuation analysis[31].

**Hilbert Statistics and Intermittency Corrections.**    Figure 4 shows the measured Hilbert-based energy spectrum $\mathcal{L}_2(f)f^{-1}$ ($\bigcirc$), where the Fourier power spectrum $E(f)$ ($\square$) is also shown for comparison. Power-law behavior is observed on the range $0.1 \leq f \leq 0.4$ day$^{-1}$ and $2 \leq f \leq 8$ day$^{-1}$ with scaling exponent $\beta_L^H = 1.59 \pm 0.08$ and $\beta_S^H = 2.89 \pm 0.07$, where $H$ presents for the Hilbert-based approach. Note that there is no half-day harmonic in the Hilbert curve since the Hilbert-based does not require harmonic to mimic the non-linear process[32]. Meanwhile, the scaling exponent $\beta_L^H$ is smaller than the one predicted by the Fourier analysis, which is an effect of the finite size sample. The measured $\beta_S^H$ is on the same level as $\beta_S^F$ provided by Fourier analysis.

The high-order scaling exponents $\zeta(q)$ are then calculated on the same scaling range for the $q$th-order Hilbert-based moments $\mathcal{L}_q(f)$ with $q$ on the range $-0.5 \leq q \leq 4$. Fig. 5 (a) shows the measured $\zeta(q)$, where the value $\zeta(q) = q/3$ (solid line) for the Kolmogorov's 1941 scaling and $\zeta(q) = q$ (dashed line) are illustrated for comparison. Visually, the measured $\zeta_L(q)$ is convex and deviates from $q/3$ when $q \geq 2$, indicating an energy-like scaling with an intermittency correction. Moreover, $\zeta_s(q)$ agrees well with $q$, implying an enstrophy-like scaling with a less intermittency correction. To compare the potential intermittency with the same reference line, the relative scaling exponent $\zeta_3^E(q)$ was calculated by fitting the measured $\mathcal{L}_q(f)$ versus $\mathcal{L}_3(f)$ on the scaling range. The measured $\zeta_3^E(q)$ is displayed in Fig. 5 (b). It confirms that the scaling behavior in the low frequency part is intermittent, while the high frequency one is less intermittent.
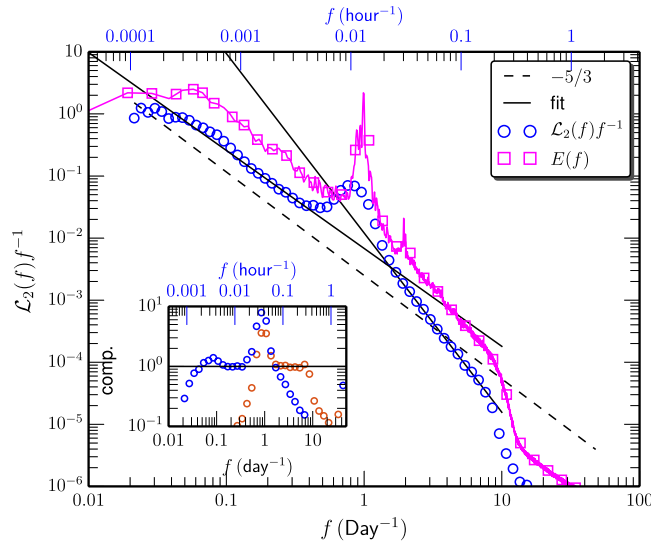
**Figure 4.** Measured Hilbert-based power spectrum $\mathcal{L}_2(f)f^{-1}$ (◯). Power-law behavior is observed on the range $0.1 \leq f \leq 0.4$ day$^{-1}$, and $2 \leq f \leq 8$ day$^{-1}$ respectively with scaling exponent $\beta_L^H = 1.59 \pm 0.08$ and $\beta_S^H = 2.89 \pm 0.07$. For comparison, the Fourier power power spectrum $E(f)$ is also shown as □. For display clarity, the spectrum curve has been vertical shifted. The inset shows the compensated curve to emphasize the observed power-law behavior. This figure is prepared using a Python package, namely Matplotlib.
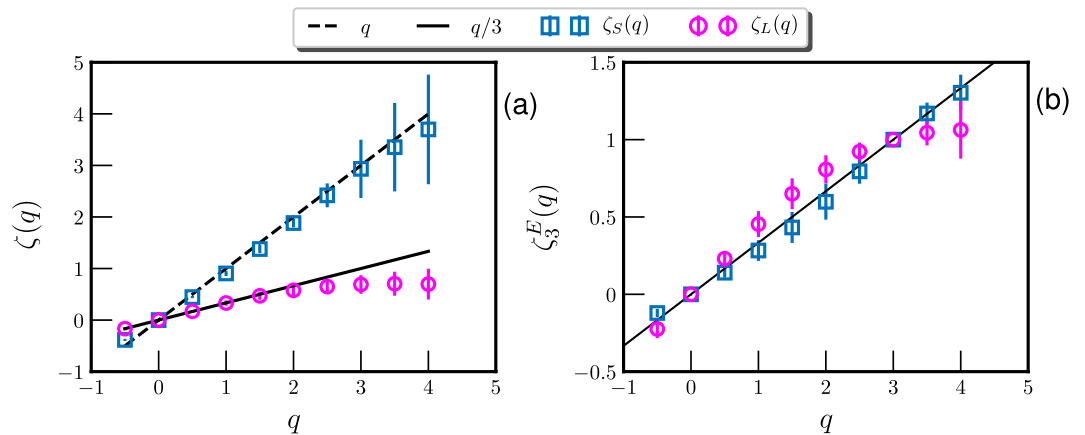


**Figure 5.** (**a**) Measured Hilbert-based scaling exponent $\zeta_S(q)$ (□) and $\zeta_L(q)$ (◯) respectively for high and low-frequency scaling ranges. For reference, $\zeta(q) = q/3$ and $\zeta(q) = q$ are shown as solid and dashed lines. (**b**) The relative scaling exponent $\zeta_3^E(q)$ by fitting the measured $\mathcal{L}_q(f)$ versus $\mathcal{L}_3(f)$. This figure is prepared using a Python package, namely Matplotlib.

## Possible Cascade Dynamics

A weak stratification with depth of $10 \sim 15$ m is reported[28]. The flow topography is thus quasi-2D. The Kraichnan's 2D turbulence picture[33] could be applied here with more complex conditions: the energy is partially injected into the system via the strong diurnal tide with a typical time scale 1 day. It is then transferred to high frequency part via a forward cascade, and transferred to low frequency part via an inverse cascade in the Lagrangian point of view. However, due to the complexity of the problem, this simple turbulence theory cannot be applied here directly to predict the scaling exponent. Another possible interpretation could be based on the so-called geostrophic turbulence[34], where the energy is injected into the system mainly via an instability of the large-scale circulation and then transferred to small scales[35]. In this situation, the scaling exponent for the large- and small-scale parts are respectively $-3$ and $-5/3$, which is on the opposite of our observation. However, to exclude any theory, a more detail examination of the scale-to-scale energy flux[36] is required to determine the direction of the cascade. It opens a new challenge to theoreticians to propose new turbulence theory in the Lagrangian frame by taking into account more facts, such as diurnal tide, stratification, earth rotation, ocean current, etc.

## Methods

**Lagrangian Drifter Data in Gulf of Mexico.** The Lagrangian drifter data is collected during the GLAD (Grand LAgrangian Deployment) observational program in the DeSoto Canyon region of the northeastern

GoM. The experiment was conducted from July to October 2012 with approximately 300 standard CODE surface drifters released over a two week period. The CODE GPS-tracked drifter is designed to follow currents in the upper 1 m with $1 - 3$ cm/s velocity errors for wind speeds up to 10 m/s[28]. The mean life-time of the drifter is around ~56 days with a standard deviation around ~27 days. According to the collected data, a stratification with $10 \sim 15$ m is observed. The same data set has been analyzed for the sub-mesoscale motion in GoM[27,28]. The GLAD drifter data used in this work is publicly available[1]. In this study, all these 300 drifters are considered.

**Autocorrelation Function and Fourier Power Spectrum.** It is often that the collected data is with different sample size for different realizations. It leads to difficulty in calculating some statistical quantities, for instance, Fourier power spectrum. In this work, two different approaches are considered. The first one is to extend the data set to have the same sample size by padding zeros to the end of the collected data. A numerical experiment shows that low frequency part will be slightly biased in this approach, for example the scaling exponent $\beta_L^F$ is slightly overestimated.

The second approach is based on the Wiener-Khinchin theorem. The autocorrelation function is firstly estimated as,

$$\rho(\tau) = \frac{1}{M(\tau)}\sum_{i=1}^{N}\widetilde{u}_i(t+\tau)\widetilde{u}_i(t) \tag{1}$$

where $\widetilde{u}(t) = u(t) - \langle u(t) \rangle_t$ is the fluctuation velocity; $\tau$ is the time lag; $N$ is the number of drifters and $M(\tau)$ is the sample size for time lag $\tau$. According to the the Wiener-Khinchin theorem, the corresponding Fourier power spectrum can be estimated via the Fourier transform,

$$E(f) = \int_{-\infty}^{+\infty} \rho(\tau)\cos(2\pi f\tau)d\tau \tag{2}$$

where $f$ is frequency. A numerical experiment shows that the high-frequency part will be biased due to the different length of trajectories, which could be suppressed via a systematical way (not employed here).

**Hilbert-Huang Transform.** To constrain the influence of the daily cycle, we employ here the so-called Hilbert-Huang transform (HHT), which is introduced by N.E Huang[32]. The first step of this methodology is to decompose a given velocity $u(t)$ data into a sum of intrinsic mode functions (IMFs) $C_i(t)$ via the so-called empirical mode decomposition (EMD) algorithm without *a priori* basis functions[32]. An IMF has to satisfy the following conditions: (i) in the whole data set, the number of extrema and the number of zero-crossings must either equal or differ at most by one and (ii) the mean value of the envelope defined by the local maxima and the envelope defined by the local minima is zero. The IMF is thus a pure oscillatory mode bearing amplitude and frequency modulations that can be extracted by the Hilbert spectral analysis[31,32] as following,

$$\widetilde{C}^A(t) = C_i(t) + j\frac{1}{\pi}P\int\frac{C_i(t')}{t-t'}dt' = \mathcal{A}_i(t)\exp(j\phi_i(t)) \tag{3}$$

where $C_i(t)$ is the extracted IMF; $j = \sqrt{-1}$; $P$ means Cauchy principle value; $\mathcal{A}_i(t)$ and $\phi_i(t)$ are amplitude function and phase function, respectively. The corresponding instantaneous frequency is then defined as,

$$f_i(t) = \frac{1}{2\pi}\frac{d\phi_i(t)}{dt} \tag{4}$$

With extracted instantaneous frequency, one can design a $f$-conditioned statistics,

$$\mathcal{L}_q(f) = \left\langle \sum_i |C_i(t)|^q|_{f_i(t)=f} \right\rangle_t \tag{5}$$

For a scaling process, one has a power-law behavior of $\mathcal{L}_q(f)$

$$\mathcal{L}_q(f) \propto f^{-\zeta(q)} \tag{6}$$

where $\zeta(q)$ is the scaling exponent[37]. Note that in this approach, the singularity transform is applied to define the analytical signal (resp. Eq. 3). Moreover, the first-order derivation of the phase function (resp. Eq. 4) is used to define the instantaneous frequency. These two steps have very local ability[31,32]. This Hilbert-based approach thus can isolate the influence of energetic structures[31,38], such as daily cycle shown here.

**Extended-Self-Similarity.** In ESS, the high-order moments are represented as a function of $p$th-order one in the power-law range to measure the scaling exponent more accurate[39], which is written as

$$\mathcal{L}_q(f) \sim \mathcal{L}_p(f)^{\zeta_p^E(q)} \tag{7}$$

where $\zeta_p^E(q)$ is a relative scaling exponent. For comparison conveniency, we consider here the third-order relative scaling exponent $\zeta_3^E(q)$ for both large and small scale parts.

# References

1. Thorpe, S. A. *The turbulent ocean* (Cambridge University Press, 2005).
2. Tennekes, H. & Lumley, J. L. *A First Course in Turbulence* (MIT Press, 1972).
3. Forristall, G. Z., Schaudt, K. J. & Cooper, C. K. Evolution and kinematics of a loop current eddy in the Gulf of Mexico during 1985. *J. Geophys. Res.* **97**, 2173–2184 (1992).
4. Oey, L.-Y., Ezer, T. & Lee, H.-C. *Circulation in the Gulf of Mexico: Observations and models*, chap. Loop Current, rings and related circulation in the Gulf of Mexico: A review of numerical models and future challenges, 31–56 (Wiley Online Library, 2005).
5. Donohue, K. *et al.* Gulf of Mexico loop current path variability. *Dynam. Atmos. Ocean* 174–194 (2016).
6. Liu, Y., Weisberg, R. H., Vignudelli, S. & Mitchum, G. T. Patterns of the loop current system and regions of sea surface height variability in the eastern Gulf of Mexico revealed by the self-organizing maps. *J. Geophys. Res.* **121**, 2347–2366 (2016).
7. Elliott, B. A. Anticyclonic rings in the Gulf of Mexico. *J. Phys. Oceanogr.* **12**, 1292–1309 (1982).
8. Vukovich, F. M. An updated evaluation of the loop current's eddy-shedding frequency. *J. Geophys. Res.* **100**, 8655–8659 (1995).
9. Sturges, W. & Leben, R. Frequency of ring separations from the loop current in the Gulf of Mexico: A revised estimate. *J. Phys. Oceanogr.* **30**, 1814–1819 (2000).
10. Leben, R. R. *Circulation in the Gulf of Mexico: Observations and models*, chap. Altimeter-Derived Loop Current Metrics, 181–201 (Wiley Online Library, 2005).
11. Dukhovskoy, D. S. *et al.* Characterization of the uncertainty of loop current metrics using a multidecadal numerical simulation and altimeter observations. *Deep Sea Res.* **100**, 140–158 (2015).
12. Lugo-Fernández, A., Leben, R. R. & Hall, C. A. Kinematic metrics of the loop current in the Gulf of Mexico from satellite altimetry. *Dynam. Atmos. Ocean* **76**, 268–282 (2016).
13. Vukovich, F. M. & Maul, G. A. Cyclonic eddies in the eastern Gulf of Mexico. *J. Phys. Oceanogr.* **15**, 105–117 (1985).
14. Zavala-Hidalgo, J., Morey, S. L. & O'Brien, J. J. Cyclonic eddies northeast of the campeche bank from altimetry data. *J. Phys. Oceanogr.* **33**, 623–629 (2003).
15. Le Hénaff, M., Kourafalou, V. H., Dussurget, R. & Lumpkin, R. Cyclonic activity in the eastern Gulf of Mexico: Characterization from along-track altimetry and *in situ* drifter trajectories. *Prog. Oceanogr.* **120**, 120–138 (2014).
16. Hofmann, E. E. & Worley, S. J. An investigation of the circulation of the Gulf of Mexico. *J. Geophys. Res.* **91**, 14221–14236 (1986).
17. Hamilton, P. Topographic rossby waves in the Gulf of Mexico. *Prog. Oceanogr.* **82**, 1–31 (2009).
18. Chérubin, L. M., Morel, Y. & Chassignet, E. P. Loop current ring shedding: The formation of cyclones and the effect of topography. *J. Phys. Oceanogr.* **36**, 569–591 (2006).
19. Donohue, K. A., Watts, D., Hamilton, P., Leben, R. & Kennelly, M. Loop current eddy formation and baroclinic instability. *Dynam. Atmos. Ocean* **76**, 195–216 (2016).
20. Oey, L. Loop current and deep eddies. *J. Phys. Oceanogr.* **38**, 1426–1449 (2008).
21. Wang, D.-P., Oey, L.-Y., Ezer, T. & Hamilton, P. Near-surface currents in Desoto Canyon (1997–99): comparison of current meters, satellite observation, and model simulation. *J. Phys. Oceanogr.* **33**, 313–326 (2003).
22. Ohlmann, J. C. & Niiler, P. P. Circulation over the continental shelf in the northern Gulf of Mexico. *Prog. Oceanogr.* **64**, 45–81 (2005).
23. Weisberg, R. H., He, R., Liu, Y. & Virmani, J. I. *Circulation in the Gulf of Mexico: Observations and models*, chap. West Florida Shelf circulation on synoptic, seasonal, and interannual time scales, 325–347 (Wiley Online Library, 2005).
24. Hamilton, P., Speer, K., Snyder, R., Wienders, N. & Leben, R. R. Shelf break exchange events near the De Soto Canyon. *Cont. Shelf Res.* **110**, 25–38 (2015).
25. Hallock, Z., Teague, W. & Jarosz, E. Subinertial slope-trapped waves in the northeastern Gulf of Mexico. *J. Phys. Oceanogr.* **39**, 1475–1485 (2009).
26. Nguyen, T.-T., Morey, S. L., Dukhovskoy, D. S. & Chassignet, E. P. Nonlocal impacts of the Loop Current on cross-slope near-bottom flow in the northeastern Gulf of Mexico. *Geophys. Res. Lett.* **42**, 2926–2933 (2015).
27. Poje, A. C. *et al.* Submesoscale dispersion in the vicinity of the deepwater horizon spill. *PNAS* **111**, 12693–12698 (2014).
28. Poje, A. C., Özgökmen, T. M., Bogucki, D. J. & Kirwan, A. Evidence of a forward energy cascade and kolmogorov self-similarity in submesoscale ocean surface drifter observations. *Phys. Fluids* **29**, 020701 (2017).
29. Landau, L. & Lifshits, E. *Fluid Mechanics* (Pergamon, London, 1987).
30. Rupolo, V. A Lagrangian-based approach for determining trajectories taxonomy and turbulence regimes. *J. Phys. Oceanogr.* **37**, 1584–1609 (2007).
31. Schmitt, F. G. & Huang, Y. *Stochastic Analysis of Scaling Time Series: From Turbulence Theory to Applications* (Cambridge Univ Press, 2016).
32. Huang, N. E. *et al.* The empirical mode decomposition and the Hilbert spectrum for nonlinear and non-stationary time series analysis. *Proc. R. Soc. London, Ser. A* **454**, 903–995 (1998).
33. Kraichnan, R. H. Inertial ranges in two-dimensional turbulence. *Phys. Fluids* **10**, 1417–1423 (1967).
34. Charney, J. G. Geostrophic turbulence. *J. Atmos. Sci.* **28**, 1087–1095 (1971).
35. Vallgren, A., Deusebio, E. & Lindborg, E. Possible explanation of the atmospheric kinetic and potential energy spectra. *Phys. Rev. Lett.* **107**, 268501 (2011).
36. Zhou, Q., Huang, Y., Lu, Z., Liu, Y. & Ni, R. Scale-to-scale energy and enstrophy transport in two-dimensional Rayleigh-Taylor turbulence. *J. Fluid Mech.* **786**, 294–308 (2015).
37. Huang, Y., Schmitt, F. G., Lu, Z. & Liu, Y. An amplitude-frequency study of turbulent scaling intermittency using Hilbert spectral analysis. *Europhys. Lett.* **84**, 40010 (2008).
38. Huang, Y. *et al.* Second-order structure function in fully developed turbulence. *Phys. Rev. E* **82**, 026319 (2010).
39. Benzi, R. *et al.* Extended self-similarity in turbulent flows. *Phys. Rev. E* **48**, 29–32 (1993).

## Acknowledgements

## Author Contributions

W.Z. and Y.H. designed this study and analyzed the data. All authors discussed the physics and contributed to the writing of the manuscript.

## Additional Information

**Competing Interests:** The authors declare that they have no competing interests.

**Publisher's note:** Springer Nature remains neutral with regard to jurisdictional claims in published maps and institutional affiliations.